

# Configuration interaction singles, time-dependent Hartree–Fock, and time-dependent density functional theory for the electronic excited states of extended systems

So Hirata

*Quantum Theory Project, University of Florida, Gainesville, Florida 32611*

Martin Head-Gordon

*Department of Chemistry, University of California, and Chemical Sciences Division, Lawrence Berkeley National Laboratory, Berkeley, California 94720*

Rodney J. Bartlett

*Quantum Theory Project, University of Florida, Gainesville, Florida 32611*

(Received 13 July 1999; accepted 28 September 1999)

A general formalism for time-dependent linear response theory is presented within the framework of linear-combination-of-atomic-orbital crystalline orbital theory for the electronic excited states of infinite one-dimensional lattices (polymers). The formalism encompasses those of time-dependent Hartree–Fock theory (TDHF), time-dependent density functional theory (TDDFT), and configuration interaction singles theory (CIS) (as the Tamm–Dancoff approximation to TDHF) as particular cases. These single-excitation theories are implemented by using a trial-vector algorithm, such that the atomic-orbital-based two-electron integrals are recomputed as needed and the transformation of these integrals from the atomic-orbital basis to the crystalline-orbital basis is avoided. Convergence of the calculated excitation energies with respect to the number of unit cells taken into account in the lattice summations ( $N$ ) and the number of wave vector sampling points ( $K$ ) is studied taking the lowest singlet and triplet exciton states of all-*trans* polyethylene as an example. The CIS and TDHF excitation energies of polyethylene show rapid convergence with respect to  $K$  and they are substantially smaller than the corresponding Hartree–Fock fundamental band gaps. In contrast, the excitation energies obtained from TDDFT and its modification, the Tamm–Dancoff approximation to TDDFT, show slower convergence with respect to  $K$  and the excitation energies to the lowest singlet exciton states tend to collapse to the corresponding Kohn–Sham fundamental band gaps in the limit of  $K \rightarrow \infty$ . We consider this to be a consequence of the incomplete cancellation of the self-interaction energy in the matrix elements of the TDDFT matrix eigenvalue equation, and to be a problem inherent to the current approximate exchange–correlation potentials that decay too rapidly in the asymptotic region. © 1999 American Institute of Physics. [S0021-9606(99)30248-8]

## I. INTRODUCTION

In many of the previous attempts to understand the electronic structures of polymeric systems, the notion of a band gap has often been invoked loosely to account for several different experimental data such as the position of optical absorption band edge, the threshold of photoemission, and the threshold of photoconduction. However, these experimental data are associated with different physical processes and should be interpreted in terms of different calculated quantities. Careful experimental studies on crystalline polymers such as those on polyethylene<sup>1–5</sup> and on polydiacetylene<sup>6–8</sup> have indeed revealed that the measured values of these quantities can be appreciably different from one another, providing a motivation to develop a quantitative theoretical method that goes beyond the simple one-electron band-structure picture. For example, the optical absorption band edge of polyethylene is located at around 7.6 eV (Refs. 1 and 3) which is lower than the observed photoemission and photoconduction threshold of 8.8 eV (Ref. 3). This result

indicates that the optical absorption bands of polyethylene below 8.8 eV correspond to the transitions to exciton states,<sup>1,3,5</sup> whose electronic structure is more suitably described as a linear combination of several singly excited configurations rather than as one configuration in which an electron is promoted from the valence band to the conduction band.

In contrast to numerous elaborate excited-state theories for molecular systems, relatively few studies have been devoted to the development of quantitative excited-state theories for polymeric systems. Among these studies are the Green's function approach to the exciton spectra of polymeric systems advocated by Suhai<sup>9–13</sup> and by Rohlffing and Louie<sup>14–16</sup> and the configuration interaction singles (CIS) and time-dependent Hartree–Fock theory (TDHF) approach to the same problem by Vračko and co-workers.<sup>17–19</sup> The Green's function approach adopted by Suhai<sup>9–13</sup> is formally equivalent to the TDHF method (or the CIS method if the Tamm–Dancoff approximation<sup>20</sup> is invoked) generalized to

extended systems when the Hartree–Fock (HF) orbitals are used as the reference orbitals. Vračko and co-workers<sup>19</sup> calculated the transition energies to the lowest exciton states of polyethylene with the CIS and TDHF methods in combination with the STO-3G and 3-21G basis sets. The excitation energies to the lowest exciton states calculated with these methods are systematically smaller than the calculated values of the HF fundamental band gap, and are considerably closer to the measured optical absorption band edge than the band gap, although they are still substantially overestimated. It has also been shown by Suhai<sup>9–13</sup> and later by others<sup>21,22</sup> that the dynamical correlation effects can be conveniently incorporated in the calculated excitation energies by using the quasiparticle energies generated from the second-order many-body perturbation calculations instead of the canonical HF orbital energies. Very recently, Rohlfing and Louie have calculated the exciton spectra of semiconductor clusters,<sup>14</sup> crystalline semiconductors and insulators,<sup>15</sup> and polymers<sup>16</sup> by solving the Bethe–Salpeter equation for the two-particle Green's function. The calculated exciton spectra were found to be in excellent quantitative agreement with the experimental results. The TDHF method (also known as the random-phase approximation, RPA) and its higher-order analogs have also been used extensively in a different context (for the calculations of polarizabilities and hyperpolarizabilities of polymers) by Champagne and co-workers<sup>23–25</sup> and recently by Otto, Gu, and Ladik.<sup>26</sup>

In view of the enormous amount of computational resources involved in the extended-system calculations, the single-excitation theories, which are the simplest excited-state theories, undoubtedly constitute the most important class of excited-state theories for extended systems. In this paper, therefore, we explore the fundamental aspects and the performance of these single-excitation theories generalized to deal with infinitely long polymeric systems. Those single-excitation theories include CIS, TDHF, and time-dependent density functional theory (TDDFT).<sup>27–30</sup> This is the same direction pursued by Suhai and Vračko and co-workers, but the present study brings about new contributions in the following three points. First, a general formalism of TDDFT is given and implemented within the framework of linear-combination-of-atomic-orbital (LCAO) crystalline orbital theory.<sup>31–35</sup> The Tamm–Dancoff approximation to TDDFT, which was proposed earlier as an algorithmically simpler alternative to TDDFT and is denoted as TDDFT/TDA,<sup>36</sup> is also implemented and studied. The general formalism given in this article also encompasses those of TDHF and CIS (as the Tamm–Dancoff approximation to TDHF) as particular cases. Second, a computationally efficient trial-vector algorithm<sup>37–41</sup> for the CIS, TDHF, TDDFT, and TDDFT/TDA methods is described and implemented. In this algorithm, an enormous amount of two-electron integrals in the atomic-orbital basis are not stored but are recomputed as needed (direct algorithm<sup>42</sup>) and the transformation of these integrals from the atomic-orbital basis to the crystalline-orbital basis is avoided. The adoption of the direct algorithm is particularly important for extended-system calculations, since the size of the integral file would easily exceed several gigabytes even for polymers with small unit cells and mod-

erate basis sets. Third, convergence of the calculated transition energies with respect to several calculation parameters is investigated and discussed. The calculation parameters include the number of unit cells taken into account in the lattice summations ( $N$ ), the number of wave vector sampling points in the first Brillouin zone ( $K$ ), and the size of basis sets. Convergence of the calculated transition energies of oligomers with respect to the chain length is also addressed.

The numerical applications are carried out for the lowest singlet and triplet exciton states of an infinite chain of all-*trans* polyethylene and its oligomers ( $n$ -alkane). In this paper, we confine ourselves to the exciton states that are accessible by the direct transitions. This treatment is justified since the wave vector of a photon is in general extremely small as compared with that of an electron and the change in the wave vector of the electron due to the excitation is negligibly small in view of the wave vector conservation law. The results obtained from the numerical applications can be summarized as follows. First, although the convergence of the excitation energies with respect to  $N$  is generally slower than that of the total energies or the band gaps, it is possible to obtain excitation energies converged up to 2 decimal places in electron volts by taking typically twice as large a value for  $N$  as that required to obtain converged total energies. The single-excitation theories based on crystalline orbital theory constitute a distinct advantage over the oligomer extrapolation method, since the excitation energies obtained by the latter method show very slow convergence, the deviations from the infinite chain limit being roughly proportional to the inverse of the chain length with a large prefactor. Second, the CIS and TDHF excitation energies converge very rapidly with respect to  $K$ , whereas the TDDFT and TDDFT/TDA excitation energies exhibit much slower convergence. We consider this slower convergence to be a consequence of the incomplete cancellation of the self-interaction energy in the matrix elements of the TDDFT and TDDFT/TDA matrix eigenvalue equation. Thus, this problem is inherent to the current approximate exchange–correlation functionals. Third, the CIS and TDHF methods yield the excitation energies to the lowest singlet exciton states that are substantially smaller than the HF fundamental band gaps, whereas the excitation energies to the lowest singlet exciton states obtained from TD-DFT and TDDFT/TDA tend to collapse to the corresponding Kohn–Sham (KS) fundamental band gaps. This is primarily due to the fact that the matrix elements of the TDDFT and TDDFT/TDA matrix eigenvalue equation are dominated by the KS orbital energy differences in the diagonal elements and the two-electron integrals which add to the diagonal and off-diagonal elements are disproportionately small. We consider this to be another manifestation of the incomplete cancellation of the self-interaction energy. The details are described in the following.

## II. THEORY

In this section, we describe the formulas of time-dependent linear response theory (Refs. 30 and 43, and references therein) for the exciton states of infinite one-dimensional lattices (polymers). The term exciton is used here in distinction to a band-to-band transition. The formal-

isms presented here assume the use of a hybrid HF/DFT functional, such that they encompass the formalisms of TDHF and TDDFT using pure exchange–correlation functionals as particular cases. The adiabatic approximation<sup>27</sup> is assumed from the outset. The CIS and TDDFT/TDA (Ref. 36) methods are defined as the Tamm–Dancoff approximation to TDHF and TDDFT, respectively, although CIS based on HF determinant is usually viewed as the lowest-order member of the hierarchical family of configuration interaction theory for excited states.

First, we assume that an infinitely long polymer is initially in a stationary state, whose electronic structure is suitably described by time-independent HF/KS theory employing periodic boundary conditions, and that the orthonormal basis functions  $\{\psi_{p\sigma}^{[k]}(\mathbf{r})\}$  are the HF/KS canonical crystalline orbitals for this unperturbed ground state, which are characterized by energy band  $p$ , spin  $\sigma$ , and wave vector  $k$ . The KS Hamiltonian (or Fock) matrix and density matrix for the ground state, which are superscripted with (0), are simply

$$F_{pq\sigma}^{(0)[k_p k_q]} = \delta_{pq} \delta_{k_p k_q} \epsilon_{p\sigma}^{[k_p]} \quad (1)$$

and

$$P_{ij\sigma}^{(0)[k_i k_j]} = \delta_{ij} \delta_{k_i k_j}, \quad (2)$$

$$P_{ia\sigma}^{(0)[k_i k_a]} = P_{a\sigma}^{(0)[k_a k_i]} = P_{ab\sigma}^{(0)[k_a k_b]} = 0, \quad (3)$$

where  $\epsilon$  are the orbital energies, and we use  $i, j$  for occupied orbitals,  $a, b$  for virtual orbitals, and  $p, q, r, s, u$  for general orbitals. These KS Hamiltonian and density matrices satisfy the time-independent HF/KS equations<sup>43</sup>

$$\sum_q \sum_{k_q}^{\text{BZ}} (F_{pq\sigma}^{(0)[k_p k_q]} P_{qr\sigma}^{(0)[k_q k_r]} - P_{pq\sigma}^{(0)[k_p k_q]} F_{qr\sigma}^{(0)[k_q k_r]}) = 0, \quad (4)$$

and the idempotency condition

$$\sum_q \sum_{k_q}^{\text{BZ}} P_{pq\sigma}^{(0)[k_p k_q]} P_{qr\sigma}^{(0)[k_q k_r]} = P_{pr\sigma}^{(0)[k_p k_r]}. \quad (5)$$

We now apply an oscillatory perturbation, which can be described as a single Fourier component,

$$G_{pq\sigma}^{[k_p k_q]} = \frac{1}{2} \{ g_{pq\sigma}^{[k_p k_q]} \exp(-i\omega t) + g_{qp\sigma}^{[k_q k_p]*} \exp(i\omega t) \}, \quad (6)$$

where the matrix  $\mathbf{g}$  represents a one-electron operator describing the details of the perturbation. The first-order (linear) response  $\mathbf{D}$  of the density matrix to this applied perturbation is

$$P_{pq\sigma}^{[k_p k_q]} = P_{pq\sigma}^{(0)[k_p k_q]} + D_{pq\sigma}^{[k_p k_q]}, \quad (7)$$

with

$$D_{pq\sigma}^{[k_p k_q]} = \frac{1}{2} \{ d_{pq\sigma}^{[k_p k_q]} \exp(-i\omega t) + d_{qp\sigma}^{[k_q k_p]*} \exp(i\omega t) \}. \quad (8)$$

The first-order change in the KS Hamiltonian matrix is composed of two terms: the change in the one-electron part described by Eq. (6) and the change in the two-electron part induced by the first-order response of the density matrix, namely,

$$F_{pq\sigma}^{[k_p k_q]} = F_{pq\sigma}^{(0)[k_p k_q]} + G_{pq\sigma}^{[k_p k_q]} + \sum_{r,s} \sum_{k_r, k_s}^{\text{BZ}} \sum_{\tau}^{\alpha, \beta} \frac{\partial F_{pq\sigma}^{[k_p k_q]}}{\partial P_{rs\tau}^{[k_r k_s]}} \Bigg|_{g=0} D_{rs\tau}^{[k_r k_s]}. \quad (9)$$

Substituting Eqs. (6) to (9) to the time-dependent HF/KS equations<sup>43</sup>

$$\sum_q \sum_{k_q}^{\text{BZ}} \{ F_{pq\sigma}^{[k_p k_q]} P_{qr\sigma}^{[k_q k_r]} - P_{pq\sigma}^{[k_p k_q]} F_{qr\sigma}^{[k_q k_r]} \} = i \frac{\partial P_{pr\sigma}^{[k_p k_r]}}{\partial t}, \quad (10)$$

and collecting the terms which are multiplied by the  $\exp(-i\omega t)$  factor, we obtain

$$\begin{aligned} & \sum_q \sum_{k_q}^{\text{BZ}} \left\{ F_{pq\sigma}^{(0)[k_p k_q]} d_{qr\sigma}^{[k_q k_r]} - d_{pq\sigma}^{[k_p k_q]} F_{qr\sigma}^{(0)[k_q k_r]} \right. \\ & \left. + \left( g_{pq\sigma}^{[k_p k_q]} + \sum_{s,u} \sum_{k_s, k_u}^{\text{BZ}} \sum_{\tau}^{\alpha, \beta} \frac{\partial F_{pq\sigma}^{[k_p k_q]}}{\partial P_{su\tau}^{[k_s k_u]}} \Bigg|_{g=0} d_{su\tau}^{[k_s k_u]} \right) \right. \\ & \left. \times P_{qr\sigma}^{(0)[k_q k_r]} - P_{pq\sigma}^{(0)[k_p k_q]} \right. \\ & \left. \times \left( g_{qr\sigma}^{[k_q k_r]} + \sum_{s,u} \sum_{k_s, k_u}^{\text{BZ}} \sum_{\tau}^{\alpha, \beta} \frac{\partial F_{qr\sigma}^{[k_q k_r]}}{\partial P_{su\tau}^{[k_s k_u]}} \Bigg|_{g=0} d_{su\tau}^{[k_s k_u]} \right) \right\} \\ & = \omega d_{pr\sigma}^{[k_p k_r]}. \quad (11) \end{aligned}$$

The terms multiplied by the  $\exp(i\omega t)$  factor lead to the complex conjugate of the above equation.

The idempotency condition

$$\sum_q \sum_{k_q}^{\text{BZ}} P_{pq\sigma}^{[k_p k_q]} P_{qr\sigma}^{[k_q k_r]} = P_{pr\sigma}^{[k_p k_r]}, \quad (12)$$

strongly restricts the possible form of the  $\mathbf{d}$  matrix in Eq. (8); the occupied–occupied and virtual–virtual elements of the  $\mathbf{d}$  matrix are zero. Rewriting

$$d_{ai\sigma}^{[k_a k_i]} = x_{ai\sigma}^{[k_a k_i]}, \quad (13)$$

$$d_{ia\sigma}^{[k_i k_a]} = y_{ia\sigma}^{[k_a k_i]}, \quad (14)$$

and using the diagonal nature of the unperturbed KS Hamiltonian and density matrices [Eqs. (1) to (3)], we obtain a pair of equations

$$\begin{aligned} & (\epsilon_{a\sigma}^{[k_a]} - \epsilon_{i\sigma}^{[k_i]}) x_{ai\sigma}^{[k_a k_i]} + g_{ai\sigma}^{[k_a k_i]} \\ & + \sum_{b,j} \sum_{k_b, k_j}^{\text{BZ}} \sum_{\tau}^{\alpha, \beta} \left( \frac{\partial F_{ai\sigma}^{[k_a k_i]}}{\partial P_{bj\tau}^{[k_b k_j]}} \Bigg|_{g=0} x_{bj\tau}^{[k_b k_j]} \right. \\ & \left. + \frac{\partial F_{ai\sigma}^{[k_a k_i]}}{\partial P_{jb\tau}^{[k_j k_b]}} \Bigg|_{g=0} y_{bj\tau}^{[k_b k_j]} \right) = \omega x_{ai\sigma}^{[k_a k_i]} \quad (15) \end{aligned}$$

and

$$\begin{aligned}
 & (\epsilon_{i\sigma}^{[k_i]} - \epsilon_{a\sigma}^{[k_a]}) y_{ai\sigma}^{[k_a k_i]} - g_{i\sigma}^{[k_i k_a]} \\
 & - \sum_{b,j} \sum_{k_b, k_j} \sum_{\tau} \left( \frac{\partial F_{ia\sigma}^{[k_i k_a]}}{\partial P_{bj\tau}^{[k_b k_j]}} \right) \Bigg|_{g=0} x_{bj\tau}^{[k_b k_j]} \\
 & + \frac{\partial F_{ia\sigma}^{[k_i k_a]}}{\partial P_{jb\tau}^{[k_j k_b]}} \Bigg|_{g=0} y_{bj\tau}^{[k_b k_j]} = \omega y_{ai\sigma}^{[k_a k_i]}. \quad (16)
 \end{aligned}$$

For a general hybrid HF/DFT functional, the KS Hamiltonian matrix elements are written explicitly as<sup>44-46</sup>

$$F_{pq\sigma}^{[k_p k_q]} = h_{pq\sigma}^{[k_p k_q]} + J_{pq\sigma}^{[k_p k_q]} - c_{\text{HF}} K_{pq\sigma}^{[k_p k_q]} + X_{pq\sigma}^{[k_p k_q]}, \quad (17)$$

with the one-electron part of the KS Hamiltonian matrix defined by

$$\begin{aligned}
 h_{pq\sigma}^{[k_p k_q]} &= \int \psi_p^{[k_p]*}(\mathbf{r}) \left( -\frac{1}{2} \nabla^2 - \sum_A \sum_n \frac{Z_A}{|\mathbf{r} - \mathbf{R}_A - n\mathbf{R}_l|} \right) \\
 & \times \psi_q^{[k_q]}(\mathbf{r}) d\mathbf{r}, \quad (18)
 \end{aligned}$$

where  $Z_A$  is the charge of nucleus  $A$  at position  $\mathbf{R}_A$  in unit cell  $n$  and  $\mathbf{R}_l$  represents the translation vector in the chain axis direction. The matrices  $\mathbf{J}$  and  $\mathbf{K}$  are the Coulomb and HF exchange contribution (with the mixing ratio of  $c_{\text{HF}}$ ), respectively, whose elements are written as

$$J_{pq\sigma}^{[k_p k_q]} = \sum_{r,s} \sum_{k_r, k_s} \sum_{\tau} (p_{\sigma}^{[k_p]} q_{\sigma}^{[k_q]} | s_{\tau}^{[k_s]} r_{\tau}^{[k_r]} ) P_{rs\tau}^{[k_r k_s]} \quad (19)$$

and

$$K_{pq\sigma}^{[k_p k_q]} = \sum_{r,s} \sum_{k_r, k_s} (p_{\sigma}^{[k_p]} r_{\sigma}^{[k_r]} | s_{\sigma}^{[k_s]} q_{\sigma}^{[k_q]} ) P_{rs\sigma}^{[k_r k_s]}, \quad (20)$$

where the two-electron integrals are written in the Mulliken notation

$$\begin{aligned}
 (p_{\sigma}^{[k_p]} q_{\sigma}^{[k_q]} | s_{\tau}^{[k_s]} r_{\tau}^{[k_r]} ) &= \int \psi_{p\sigma}^{[k_p]*}(\mathbf{r}) \psi_{q\sigma}^{[k_q]}(\mathbf{r}) \frac{1}{|\mathbf{r} - \mathbf{r}'|} \\
 & \times \psi_{s\tau}^{[k_s]*}(\mathbf{r}') \psi_{r\tau}^{[k_r]}(\mathbf{r}') d\mathbf{r} d\mathbf{r}'. \quad (21)
 \end{aligned}$$

The last term in Eq. (17) is the contribution from the exchange–correlation functional, and is written as<sup>46-48</sup>

$$\begin{aligned}
 X_{pq\alpha}^{[k_p k_q]} &= \int \left\{ \frac{\partial f}{\partial \rho_{\alpha}} \psi_{p\alpha}^{[k_p]*} \psi_{q\alpha}^{[k_q]} \right. \\
 & \left. + \left( 2 \frac{\partial f}{\partial \gamma_{\alpha\alpha}} \nabla \rho_{\alpha} + \frac{\partial f}{\partial \gamma_{\alpha\beta}} \nabla \rho_{\beta} \right) \cdot \nabla (\psi_{p\alpha}^{[k_p]*} \psi_{q\alpha}^{[k_q]}) \right\} d\mathbf{r}, \quad (22)
 \end{aligned}$$

and similarly for the  $\beta$  spin counterpart. Here  $f$  is a sum of appropriately scaled exchange–correlation functionals of spin densities  $\rho_{\alpha}, \rho_{\beta}$  and gradient invariants  $\gamma_{\alpha\alpha}, \gamma_{\alpha\beta}, \gamma_{\beta\beta}$ . The spin density  $\rho_{\sigma}(\mathbf{r})$  is related to the density matrix by

$$\rho_{\sigma}(\mathbf{r}) = \sum_{p,q} \sum_{k_p, k_q} P_{pq\sigma}^{[k_p k_q]} \psi_{p\sigma}^{[k_p]}(\mathbf{r}) \psi_{q\sigma}^{[k_q]*}(\mathbf{r}). \quad (23)$$

Using the above definitions, we find<sup>49,50</sup>

$$\begin{aligned}
 & \frac{\partial F_{pq\sigma}^{[k_p k_q]}}{\partial P_{rs\tau}^{[k_r k_s]}} \Bigg|_{g=0} \\
 &= (p_{\sigma}^{[k_p]} q_{\sigma}^{[k_q]} | s_{\tau}^{[k_s]} r_{\tau}^{[k_r]} ) - c_{\text{HF}} \delta_{\sigma\tau} (p_{\sigma}^{[k_p]} r_{\tau}^{[k_r]} | s_{\tau}^{[k_s]} q_{\sigma}^{[k_q]} ) \\
 & + (p_{\sigma}^{[k_p]} q_{\sigma}^{[k_q]} | w_{\sigma\tau} | s_{\tau}^{[k_s]} r_{\tau}^{[k_r]} ), \quad (24)
 \end{aligned}$$

with

$$\begin{aligned}
 (p_{\alpha}^{[k_p]} q_{\alpha}^{[k_q]} | w_{\alpha\alpha} | s_{\alpha}^{[k_s]} r_{\alpha}^{[k_r]} ) &= 2 \int \nabla (\psi_{p\alpha}^{[k_p]*} \psi_{q\alpha}^{[k_q]}) \cdot \nabla (\psi_{s\alpha}^{[k_s]*} \psi_{r\alpha}^{[k_r]}) \frac{\partial f}{\partial \gamma_{\alpha\alpha}} d\mathbf{r} + \int \psi_{p\alpha}^{[k_p]*} \psi_{q\alpha}^{[k_q]} \frac{\partial^2 f}{\partial \rho_{\alpha}^2} \psi_{s\alpha}^{[k_s]*} \psi_{r\alpha}^{[k_r]} d\mathbf{r} + 2 \int \psi_{p\alpha}^{[k_p]*} \psi_{q\alpha}^{[k_q]} \\
 & \times \frac{\partial^2 f}{\partial \rho_{\alpha} \partial \gamma_{\alpha\alpha}} \nabla \rho_{\alpha} \cdot \nabla (\psi_{s\alpha}^{[k_s]*} \psi_{r\alpha}^{[k_r]}) d\mathbf{r} + 2 \int \nabla \rho_{\alpha} \cdot \nabla (\psi_{p\alpha}^{[k_p]*} \psi_{q\alpha}^{[k_q]}) \frac{\partial^2 f}{\partial \rho_{\alpha} \partial \gamma_{\alpha\alpha}} \psi_{s\alpha}^{[k_s]*} \psi_{r\alpha}^{[k_r]} d\mathbf{r} \\
 & + \int \nabla \rho_{\beta} \cdot \nabla (\psi_{p\alpha}^{[k_p]*} \psi_{q\alpha}^{[k_q]}) \frac{\partial^2 f}{\partial \rho_{\alpha} \partial \gamma_{\alpha\beta}} \psi_{s\alpha}^{[k_s]*} \psi_{r\alpha}^{[k_r]} d\mathbf{r} + \int \psi_{p\alpha}^{[k_p]*} \psi_{q\alpha}^{[k_q]} \\
 & \times \frac{\partial^2 f}{\partial \rho_{\alpha} \partial \gamma_{\alpha\beta}} \nabla \rho_{\beta} \cdot \nabla (\psi_{s\alpha}^{[k_s]*} \psi_{r\alpha}^{[k_r]}) d\mathbf{r} + 4 \int \nabla \rho_{\alpha} \cdot \nabla (\psi_{p\alpha}^{[k_p]*} \psi_{q\alpha}^{[k_q]}) \frac{\partial^2 f}{\partial \gamma_{\alpha\alpha}^2} \nabla \rho_{\alpha} \cdot \nabla (\psi_{s\alpha}^{[k_s]*} \psi_{r\alpha}^{[k_r]}) d\mathbf{r} \\
 & + 2 \int \nabla \rho_{\alpha} \cdot \nabla (\psi_{p\alpha}^{[k_p]*} \psi_{q\alpha}^{[k_q]}) \frac{\partial^2 f}{\partial \gamma_{\alpha\alpha} \partial \gamma_{\alpha\beta}} \nabla \rho_{\beta} \cdot \nabla (\psi_{s\alpha}^{[k_s]*} \psi_{r\alpha}^{[k_r]}) d\mathbf{r} \\
 & + 2 \int \nabla \rho_{\beta} \cdot \nabla (\psi_{p\alpha}^{[k_p]*} \psi_{q\alpha}^{[k_q]}) \frac{\partial^2 f}{\partial \gamma_{\alpha\alpha} \partial \gamma_{\alpha\beta}} \nabla \rho_{\alpha} \cdot \nabla (\psi_{s\alpha}^{[k_s]*} \psi_{r\alpha}^{[k_r]}) d\mathbf{r} \\
 & + \int \nabla \rho_{\beta} \cdot \nabla (\psi_{p\alpha}^{[k_p]*} \psi_{q\alpha}^{[k_q]}) \frac{\partial^2 f}{\partial \gamma_{\alpha\beta}^2} \nabla \rho_{\beta} \cdot \nabla (\psi_{s\alpha}^{[k_s]*} \psi_{r\alpha}^{[k_r]}) d\mathbf{r}, \quad (25)
 \end{aligned}$$

and

$$\begin{aligned}
(p_{\alpha}^{[k_p]} q_{\alpha}^{[k_q]} | w_{\alpha\beta} | s_{\beta}^{[k_s]} r_{\beta}^{[k_r]}) = & \int \nabla(\psi_{p\alpha}^{[k_p]*} \psi_{q\alpha}^{[k_q]}) \cdot \nabla(\psi_{s\beta}^{[k_s]*} \psi_{r\beta}^{[k_r]}) \frac{\partial f}{\partial \gamma_{\alpha\beta}} d\mathbf{r} + \int \psi_{p\alpha}^{[k_p]*} \psi_{q\alpha}^{[k_q]} \frac{\partial^2 f}{\partial \rho_{\alpha} \partial \rho_{\beta}} \psi_{s\beta}^{[k_s]*} \psi_{r\beta}^{[k_r]} d\mathbf{r} \\
& + 2 \int \psi_{p\alpha}^{[k_p]*} \psi_{q\alpha}^{[k_q]} \frac{\partial^2 f}{\partial \rho_{\alpha} \partial \gamma_{\beta\beta}} \nabla \rho_{\beta} \cdot \nabla(\psi_{s\beta}^{[k_s]*} \psi_{r\beta}^{[k_r]}) d\mathbf{r} + 2 \int \nabla \rho_{\alpha} \cdot \nabla(\psi_{p\alpha}^{[k_p]*} \psi_{q\alpha}^{[k_q]}) \\
& \times \frac{\partial^2 f}{\partial \rho_{\beta} \partial \gamma_{\alpha\alpha}} \psi_{s\beta}^{[k_s]*} \psi_{r\beta}^{[k_r]} d\mathbf{r} + \int \psi_{p\alpha}^{[k_p]*} \psi_{q\alpha}^{[k_q]} \frac{\partial^2 f}{\partial \rho_{\alpha} \partial \gamma_{\alpha\beta}} \nabla \rho_{\alpha} \cdot \nabla(\psi_{s\beta}^{[k_s]*} \psi_{r\beta}^{[k_r]}) d\mathbf{r} \\
& + \int \nabla \rho_{\beta} \cdot \nabla(\psi_{p\alpha}^{[k_p]*} \psi_{q\alpha}^{[k_q]}) \frac{\partial^2 f}{\partial \rho_{\beta} \partial \gamma_{\alpha\beta}} \psi_{s\beta}^{[k_s]*} \psi_{r\beta}^{[k_r]} d\mathbf{r} + 4 \int \nabla \rho_{\alpha} \cdot \nabla(\psi_{p\alpha}^{[k_p]*} \psi_{q\alpha}^{[k_q]}) \\
& \times \frac{\partial^2 f}{\partial \gamma_{\alpha\alpha} \partial \gamma_{\beta\beta}} \nabla \rho_{\beta} \cdot \nabla(\psi_{s\beta}^{[k_s]*} \psi_{r\beta}^{[k_r]}) d\mathbf{r} + 2 \int \nabla \rho_{\alpha} \cdot \nabla(\psi_{p\alpha}^{[k_p]*} \psi_{q\alpha}^{[k_q]}) \frac{\partial^2 f}{\partial \gamma_{\alpha\alpha} \partial \gamma_{\alpha\beta}} \nabla \rho_{\alpha} \cdot \nabla(\psi_{s\beta}^{[k_s]*} \psi_{r\beta}^{[k_r]}) d\mathbf{r} \\
& + 2 \int \nabla \rho_{\beta} \cdot \nabla(\psi_{p\alpha}^{[k_p]*} \psi_{q\alpha}^{[k_q]}) \frac{\partial^2 f}{\partial \gamma_{\beta\beta} \partial \gamma_{\alpha\beta}} \nabla \rho_{\beta} \cdot \nabla(\psi_{s\beta}^{[k_s]*} \psi_{r\beta}^{[k_r]}) d\mathbf{r} + \int \nabla \rho_{\beta} \cdot \nabla(\psi_{p\alpha}^{[k_p]*} \psi_{q\alpha}^{[k_q]}) \\
& \times \frac{\partial^2 f}{\partial \gamma_{\alpha\beta}^2} \nabla \rho_{\alpha} \cdot \nabla(\psi_{s\beta}^{[k_s]*} \psi_{r\beta}^{[k_r]}) d\mathbf{r}. \tag{26}
\end{aligned}$$

The  $\beta\beta$  and  $\beta\alpha$  matrix elements are readily obtained by interchanging  $\alpha$  and  $\beta$  in the above equations wherever they appear.

Substituting Eq. (24) into Eqs. (15) and (16) and assuming that the electronic transitions occur with an infinitesimal perturbation ( $g_{ia\sigma}^{[k_i k_a]} = g_{ai\sigma}^{[k_a k_i]} = 0$ ), we obtain a non-Hermitian eigenvalue equation

$$\begin{pmatrix} \mathbf{A} & \mathbf{B} \\ \mathbf{B}^* & \mathbf{A}^* \end{pmatrix} \begin{pmatrix} \mathbf{X} \\ \mathbf{Y} \end{pmatrix} = \omega \begin{pmatrix} \mathbf{1} & \mathbf{0} \\ \mathbf{0} & -\mathbf{1} \end{pmatrix} \begin{pmatrix} \mathbf{X} \\ \mathbf{Y} \end{pmatrix}, \tag{27}$$

with

$$\begin{aligned}
A_{ai\sigma, bj\tau}^{[k_a k_i, k_b k_j]} = & \delta_{ij} \delta_{ab} \delta_{k_i k_j} \delta_{a k_b} \delta_{\sigma\tau} (\epsilon_{a\sigma}^{[k_a]} - \epsilon_{i\tau}^{[k_i]}) \\
& + (a_{\sigma}^{[k_a]; [k_i]} | j_{\tau}^{[k_j]} b_{\tau}^{[k_b]} ) \\
& - c_{\text{HF}} \delta_{\sigma\tau} (a_{\sigma}^{[k_a]} b_{\tau}^{[k_b]} | j_{\tau}^{[k_j]} i_{\sigma}^{[k_i]} ) \\
& + (a_{\sigma}^{[k_a]} i_{\sigma}^{[k_i]} | w_{\sigma\tau} | j_{\tau}^{[k_j]} b_{\tau}^{[k_b]} ), \tag{28}
\end{aligned}$$

$$\begin{aligned}
B_{ai\sigma, bj\tau}^{[k_a k_i, k_b k_j]} = & (a_{\sigma}^{[k_a]; [k_i]} | b_{\tau}^{[k_b]} j_{\tau}^{[k_j]} ) \\
& - c_{\text{HF}} \delta_{\sigma\tau} (a_{\sigma}^{[k_a]} j_{\tau}^{[k_j]} | b_{\tau}^{[k_b]} i_{\sigma}^{[k_i]} ) \\
& + (a_{\sigma}^{[k_a]} i_{\sigma}^{[k_i]} | w_{\sigma\tau} | b_{\tau}^{[k_b]} j_{\tau}^{[k_j]} ). \tag{29}
\end{aligned}$$

At this point, we exploit the fact that the two-electron integrals appearing in Eqs. (28) and (29) vanish identically unless  $(-k_a + k_i - k_j + k_b)$  is an integral multiple of  $2\pi/R_i$  (Refs. 9–13 and 17–19). This means that the  $\mathbf{A}$  and  $\mathbf{B}$  matrices in Eq. (27) have nonzero elements only within the blocks whose wave vector indexes satisfy the following condition:

$$k_a - k_i = k_b - k_j + \frac{2m\pi}{R_i} \equiv \Delta k, \tag{30}$$

where  $m$  is an integer. Therefore, the large matrix eigenvalue problem (27)–(29) can be decomposed into smaller matrix

eigenvalue problems, and each smaller eigenvalue problem is characterized by the exciton wavevector  $\Delta k$  introduced in the above equation. The matrix equation to be solved for a given  $\Delta k$  has apparently the same form (27) as before, but the  $\mathbf{A}$  and  $\mathbf{B}$  matrix elements are now defined by

$$\begin{aligned}
A_{ai\sigma, bj\tau}^{[k_i, k_j]} = & \delta_{ij} \delta_{ab} \delta_{k_i k_j} \delta_{\sigma\tau} (\epsilon_{a\sigma}^{[k_i + \Delta k]} - \epsilon_{i\tau}^{[k_i]}) \\
& + (a_{\sigma}^{[k_i + \Delta k]; [k_i]} | j_{\tau}^{[k_j]} b_{\tau}^{[k_j + \Delta k]} ) \\
& - c_{\text{HF}} \delta_{\sigma\tau} (a_{\sigma}^{[k_i + \Delta k]} b_{\tau}^{[k_j + \Delta k]} | j_{\tau}^{[k_j]} i_{\sigma}^{[k_i]} ) \\
& + (a_{\sigma}^{[k_i + \Delta k]; [k_i]} | w_{\sigma\tau} | j_{\tau}^{[k_j]} b_{\tau}^{[k_j + \Delta k]} ), \tag{31}
\end{aligned}$$

$$\begin{aligned}
B_{ai\sigma, bj\tau}^{[k_i, k_j]} = & (a_{\sigma}^{[k_i + \Delta k]; [k_i]} | b_{\tau}^{[k_j + \Delta k]} j_{\tau}^{[k_j]} ) \\
& - c_{\text{HF}} \delta_{\sigma\tau} (a_{\sigma}^{[k_i + \Delta k]} j_{\tau}^{[k_j]} | b_{\tau}^{[k_j + \Delta k]} i_{\sigma}^{[k_i]} ) \\
& + (a_{\sigma}^{[k_i + \Delta k]; [k_i]} | w_{\sigma\tau} | b_{\tau}^{[k_j + \Delta k]} j_{\tau}^{[k_j]} ). \tag{32}
\end{aligned}$$

Note that the dimension of the  $\mathbf{A}$  and  $\mathbf{B}$  matrices of Eqs. (31) and (32) is smaller by a factor of  $K^2$  than those of Eqs. (28) and (29) with  $K$  being the number of wave vector sampling points. For the direct transitions ( $\Delta k = 0$ ), the definition of the  $\mathbf{A}$  and  $\mathbf{B}$  matrices is further simplified to

$$\begin{aligned}
A_{ai\sigma, bj\tau}^{[k_i, k_j]} = & \delta_{ij} \delta_{ab} \delta_{k_i k_j} \delta_{\sigma\tau} (\epsilon_{a\sigma}^{[k_i]} - \epsilon_{i\tau}^{[k_i]}) \\
& + (a_{\sigma}^{[k_i]; [k_i]} | j_{\tau}^{[k_j]} b_{\tau}^{[k_j]} ) \\
& - c_{\text{HF}} \delta_{\sigma\tau} (a_{\sigma}^{[k_i]} b_{\tau}^{[k_j]} | j_{\tau}^{[k_j]} i_{\sigma}^{[k_i]} ) \\
& + (a_{\sigma}^{[k_i]; [k_i]} | w_{\sigma\tau} | j_{\tau}^{[k_j]} b_{\tau}^{[k_j]} ), \tag{33}
\end{aligned}$$

$$\begin{aligned}
B_{ai\sigma, bj\tau}^{[k_i, k_j]} = & (a_{\sigma}^{[k_i]; [k_i]} | b_{\tau}^{[k_j]} j_{\tau}^{[k_j]} ) \\
& - c_{\text{HF}} \delta_{\sigma\tau} (a_{\sigma}^{[k_i]} j_{\tau}^{[k_j]} | b_{\tau}^{[k_j]} i_{\sigma}^{[k_i]} ) \\
& + (a_{\sigma}^{[k_i]; [k_i]} | w_{\sigma\tau} | b_{\tau}^{[k_j]} j_{\tau}^{[k_j]} ). \tag{34}
\end{aligned}$$

Equations (27), (33), and (34) are solved to obtain excitation energies  $\omega$  of TDHF or TDDFT. The Tamm–Dancoff approximation<sup>20</sup> amounts to substituting zero for the  $\mathbf{B}$  matrix elements in Eq. (27), which leads to a simpler Hermitian eigenvalue problem of the form

$$\mathbf{A}\mathbf{X} = \omega\mathbf{X}, \quad (35)$$

where the definition of the  $\mathbf{A}$  matrix elements is the same as before [Eqs. (31) and (33)]. The eigenvalues  $\omega$  correspond to the excitation energies of CIS or TDDFT/TDA.

### III. IMPLEMENTATION

In HF/KS crystalline orbital theory, each canonical crystalline (Bloch) orbital is expressed as a linear combination of atomic orbitals  $\{\chi_\mu^{(n)}(\mathbf{r})\}$  in the form

$$\psi_{p\sigma}^{[k_p]}(\mathbf{r}) = K^{-1/2} \sum_{\mu} \sum_n C_{\mu p \sigma}^{[k_p]} \exp(ink_p R_l) \chi_\mu^{(n)}(\mathbf{r}), \quad (36)$$

where  $K$  is the number of wave vector sampling points in the first Brillouin zone. The atomic orbital  $\chi_\mu^{(n)}(\mathbf{r})$  is a real spatial function centered in unit cell  $n$ . The two-electron integrals over the canonical crystalline orbitals are written in terms of the atomic orbitals as

$$\begin{aligned} & (p_\sigma^{[k_p]} q_\sigma^{[k_q]} | s_\tau^{[k_s]} r_\tau^{[k_r]}) \\ &= K^{-1} \sum_{\mu, \nu, \lambda, \kappa} \sum_{l, m, n} C_{\mu p \sigma}^{[k_p]*} C_{\nu q \sigma}^{[k_q]*} C_{\lambda s \tau}^{[k_s]*} C_{\kappa r \tau}^{[k_r]*} \\ & \quad \times \exp\{i(k_q l - k_s m + k_r n) R_l\} (\mu^{(0)} \nu^{(l)} | \lambda^{(m)} \kappa^{(n)}), \quad (37) \end{aligned}$$

when the condition (30) is satisfied; otherwise the integrals vanish. The two-electron integrals over the atomic orbitals are written as

$$\begin{aligned} & (\mu^{(0)} \nu^{(l)} | \lambda^{(m)} \kappa^{(n)}) \\ &= \int \chi_\mu^{(0)}(\mathbf{r}) \chi_\nu^{(l)}(\mathbf{r}) \frac{1}{|\mathbf{r} - \mathbf{r}'|} \chi_\lambda^{(m)}(\mathbf{r}') \chi_\kappa^{(n)}(\mathbf{r}') d\mathbf{r} d\mathbf{r}'. \quad (38) \end{aligned}$$

Likewise the two-electron integrals over the canonical crystalline orbitals involving the electric second derivatives of exchange–correlation functionals vanish unless the condition (30) is satisfied. Nonvanishing integrals are related to the two-electron integrals over the atomic orbitals as

$$\begin{aligned} & (p_\sigma^{[k_p]} q_\sigma^{[k_q]} | w_{\sigma\tau} | s_\tau^{[k_s]} r_\tau^{[k_r]}) \\ &= K^{-1} \sum_{\mu, \nu, \lambda, \kappa} \sum_{l, m, n} C_{\mu p \sigma}^{[k_p]*} C_{\nu q \sigma}^{[k_q]*} C_{\lambda s \tau}^{[k_s]*} C_{\kappa r \tau}^{[k_r]*} \\ & \quad \times \exp\{i(k_q l - k_s m + k_r n) R_l\} (\mu^{(0)} \nu^{(l)} | w_{\sigma\tau} | \lambda^{(m)} \kappa^{(n)}), \quad (39) \end{aligned}$$

where the definition of the two-electron integrals over the atomic orbitals can be readily inferred from Eqs. (25) and (26), and is not given here.

In the present implementation of TDHF and TDDFT, the explicit formation of an enormous number of these two-electron integrals over crystalline orbitals is avoided by invoking a trial-vector algorithm,<sup>37</sup> which is based on the idea of projecting the full matrices onto ones of greatly reduced

dimensions.<sup>51,52</sup> The generalization of this algorithm to a non-Hermitian eigenvalue equation has been considered by Hirao and Nakatsuji<sup>53</sup> and for the particular form of Eq. (27) by Olsen, Jensen, and Jørgensen.<sup>38</sup> It should be remembered that the  $\mathbf{A}$  and  $\mathbf{B}$  matrices are complex matrices and hence we cannot reduce Eq. (27) to a Hermitian eigenvalue equation of half the dimension as has usually been done in the implementations for molecules.<sup>36,41,49,50,54,55</sup> The CIS and TDDFT/TDA methods can be implemented with minor modification to this algorithm outlined below. In the Olsen algorithm, the  $\mathbf{A}$  and  $\mathbf{B}$  matrices in Eq. (27) are projected onto a subspace spanned by a set of trial vectors  $\{(\mathbf{x}^{(1)}, \mathbf{y}^{(1)}), (\mathbf{x}^{(2)}, \mathbf{y}^{(2)}), \dots, (\mathbf{x}^{(n)}, \mathbf{y}^{(n)})\}$ . Each iteration involves the formation of matrix–trial vector products

$$\bar{x}_{ai\sigma}^{(p)} = \sum_{j,b} \sum_{\tau}^{\alpha,\beta} (A_{ai\sigma,bj\tau} x_{bj\tau}^{(p)} + B_{ai\sigma,bj\tau} y_{bj\tau}^{(p)}), \quad (40)$$

$$\bar{y}_{ai\sigma}^{(p)} = \sum_{j,b} \sum_{\tau}^{\alpha,\beta} (B_{ai\sigma,bj\tau}^* x_{bj\tau}^{(p)} + A_{ai\sigma,bj\tau}^* y_{bj\tau}^{(p)}). \quad (41)$$

The subspace representation of the  $\mathbf{A}$  and  $\mathbf{B}$  matrices, denoted as  $\mathbf{A}'$  and  $\mathbf{B}'$ , is obtained by forming the inner product of the trial vectors and the product vectors

$$A'_{pq} = \sum_{i,a} \sum_{\sigma}^{\alpha,\beta} (x_{ai\sigma}^{(p)*} \bar{x}_{ai\sigma}^{(q)} + y_{ai\sigma}^{(p)*} \bar{y}_{ai\sigma}^{(q)}), \quad (42)$$

$$B'_{pq} = \sum_{i,a} \sum_{\sigma}^{\alpha,\beta} (x_{ai\sigma}^{(p)*} \bar{y}_{ai\sigma}^{(q)*} + y_{ai\sigma}^{(p)*} \bar{x}_{ai\sigma}^{(q)*}). \quad (43)$$

Likewise the subspace representation of the metric is obtained as

$$C'_{pq} = \sum_{i,a} \sum_{\sigma}^{\alpha,\beta} (x_{ai\sigma}^{(p)*} x_{ai\sigma}^{(q)} - y_{ai\sigma}^{(p)*} y_{ai\sigma}^{(q)}), \quad (44)$$

$$D'_{pq} = \sum_{i,a} \sum_{\sigma}^{\alpha,\beta} (x_{ai\sigma}^{(p)*} y_{ai\sigma}^{(q)*} - y_{ai\sigma}^{(p)*} x_{ai\sigma}^{(q)*}). \quad (45)$$

These matrices satisfy the following relations:

$$A'_{pq} = A'_{qp*}, \quad (46)$$

$$B'_{pq} = B'_{qp}, \quad (47)$$

$$C'_{pq} = C'_{qp*}, \quad (48)$$

$$D'_{pq} = -D'_{qp}. \quad (49)$$

The approximate eigenvalues  $\omega'$  are obtained by solving the non-Hermitian eigenvalue equation of the reduced dimension

$$\begin{pmatrix} \mathbf{A}' & \mathbf{B}' \\ \mathbf{B}'^* & \mathbf{A}'^* \end{pmatrix} \begin{pmatrix} \mathbf{X}' \\ \mathbf{Y}' \end{pmatrix} = \omega' \begin{pmatrix} \mathbf{C}' & \mathbf{D}' \\ -\mathbf{D}'^* & -\mathbf{C}'^* \end{pmatrix} \begin{pmatrix} \mathbf{X}' \\ \mathbf{Y}' \end{pmatrix}. \quad (50)$$

Subspace size is increased iteratively until the approximate eigenvalues  $\omega'$  converge within the preset tolerance. The non-Hermitian eigenvalue problem (50) can be viewed as a Hermitian eigenvalue problem by considering the matrix in the left-hand side, which is positive definite for the ground state,<sup>56</sup> as metric and  $1/\omega'$  as eigenvalues. Thus this matrix equation can be solved by standard algorithms. Care must be

exercised to ensure that the trial vectors employed in each iteration are linearly independent,<sup>51,52</sup> since the subspace method described above implicitly uses trial vectors of the form  $\{(\mathbf{y}^{(1)*}, \mathbf{x}^{(1)*}), (\mathbf{y}^{(2)*}, \mathbf{x}^{(2)*}), \dots, (\mathbf{y}^{(n)*}, \mathbf{x}^{(n)*})\}$  also. In our implementation, we diagonalize the metric of these trial vectors every time a new trial vector is added, and verify that the new vector does not introduce linear dependence in the subspace.

The formation of matrix-trial vector products can be carried out conveniently in the direct atomic-orbital-based algorithm, which is illustrated in the following for the product formation of a trial vector and the two-electron integrals involving the electric second derivative of a local exchange-correlation functional, namely,

$$\begin{aligned} & \sum_{j,b} \sum_{k_j} \sum_{\tau}^{\text{BZ } \alpha,\beta} (a_{\sigma}^{[k_i]} i_{\sigma}^{[k_i]} | w_{\sigma\tau} | j_{\tau}^{[k_j]} b_{\tau}^{[k_j]}) x_{bj\tau}^{(p)} \\ &= K^{-1} \sum_{j,b} \sum_{k_j} \sum_{\tau}^{\text{BZ } \alpha,\beta} \sum_{\mu,\nu,\lambda,\kappa} \sum_{l,m,n} x_{bj\tau}^{(p)} C_{\mu\alpha\sigma}^{[k_i]*} C_{\nu i\sigma}^{[k_i]*} C_{\lambda j\tau}^{[k_j]*} C_{\kappa b\tau}^{[k_j]} \\ & \quad \times \exp\{i(k_i l - k_j m + k_j n) R_i\} \\ & \quad \times \int \chi_{\mu}^{(0)}(\mathbf{r}) \chi_{\nu}^{(l)}(\mathbf{r}) \frac{\partial^2 f}{\partial \rho_{\sigma} \partial \rho_{\tau}} \chi_{\lambda}^{(m)}(\mathbf{r}) \chi_{\kappa}^{(n)}(\mathbf{r}) d\mathbf{r}. \quad (51) \end{aligned}$$

The summation can be carried out in four separate steps. First, we form a density-matrix-like quantity (which we call trial density matrix) defined by

$$T_{\lambda\kappa\tau}^{(n-m)} = K^{-1} \sum_{j,b} \sum_{k_j}^{\text{BZ}} x_{bj\tau}^{(p)} C_{\lambda j\tau}^{[k_j]*} C_{\kappa b\tau}^{[k_j]} \exp\{i k_j (n-m) R_i\}. \quad (52)$$

Second, we form an electron-density-like quantity (and their gradients and gradient invariants with respect to the electric variables if a gradient-corrected functional is being used) at each point of the numerical integration grid

$$\rho_{\tau}^T(\mathbf{r}) = \sum_{\lambda,\kappa} \sum_{m,n} T_{\lambda\kappa\tau}^{(n-m)} \chi_{\lambda}^{(m)}(\mathbf{r}) \chi_{\kappa}^{(n)}(\mathbf{r}). \quad (53)$$

Third, we carry out numerical integration to obtain

$$S_{\mu\nu\sigma}^{(l)} = \sum_{\tau}^{\alpha,\beta} \int \chi_{\mu}^{(0)}(\mathbf{r}) \chi_{\nu}^{(l)}(\mathbf{r}) \frac{\partial^2 f}{\partial \rho_{\sigma} \partial \rho_{\tau}} \rho_{\tau}^T(\mathbf{r}) d\mathbf{r}. \quad (54)$$

The computational cost of this process for one trial vector is on the same order of that of forming the exchange-correlation contributions to KS Hamiltonian matrix elements in the ground-state DFT calculations, because the above equation involves only two atomic-orbital indexes. Finally, we backtransform this atomic-orbital-based product vector to that over the crystalline orbitals

$$\begin{aligned} & \sum_{j,b} \sum_{k_j} \sum_{\tau}^{\text{BZ } \alpha,\beta} (a_{\sigma}^{[k_i]} i_{\sigma}^{[k_i]} | w_{\sigma\tau} | j_{\tau}^{[k_j]} b_{\tau}^{[k_j]}) x_{bj\tau}^{(p)} \\ &= \sum_{\mu,\nu} \sum_l C_{\mu\alpha\sigma}^{[k_i]*} C_{\nu i\sigma}^{[k_i]*} \exp(ik_i l R_i) S_{\mu\nu\sigma}^{(l)}. \quad (55) \end{aligned}$$

The single-excitation theories outlined in this and previous sections have been implemented in the POLYMER pro-

gram package,<sup>57</sup> the details of which were described in our previous articles.<sup>45,46,58-61</sup> We employed the Slater-Vosko-Wilk-Nusair (SVWN),<sup>62,63</sup> Becke-Lee-Yang-Parr (BLYP),<sup>64,65</sup> and Becke3-Lee-Yang-Parr (B3LYP)<sup>66</sup> functionals as representative local, gradient-corrected, and hybrid functionals, respectively, in TDDFT and TDDFT/TDA calculations. The CIS, TDHF, TDDFT, and TDDFT/TDA calculations on oligomers (*n*-alkane molecules) were carried out using a development version of the Q-CHEM program package.<sup>67</sup>

#### IV. NUMERICAL APPLICATION

First, we briefly address the cutoff criterion of two-electron integrals employed in this study, which seems to be particularly relevant to the following discussions. We employed the so-called 'Namur cutoff criterion' for truncating the infinite lattice summations (see Ref. 68 for the performance of various cutoff criteria), which was advocated by Delhalle *et al.*<sup>69</sup> This criterion uses two parameters *M* and *N*, and the two-electron integrals over the atomic orbitals whose unit cell indexes are in a certain range determined by these parameters are computed and included in the lattice summations. Specifically, we compute the two-electron integrals of the form  $(\mu^{(0)} \nu^{(l)} | \lambda^{(m)} \kappa^{(n)})$  with the unit cell indexes in the range

$$-M < l < +M, \quad (56)$$

$$-N < m < +N, \quad (57)$$

$$m - M < n < m + M. \quad (58)$$

It is easy to obtain converged results with respect to parameter *M*, since the two-electron integrals decay exponentially with increasing the distance between the atomic orbitals  $\mu^{(0)}$  and  $\nu^{(l)}$  or that between  $\lambda^{(m)}$  and  $\kappa^{(n)}$ . In contrast, the convergence of the results with respect to parameter *N* is generally much slower since the two-electron integrals may decay asymptotically in inverse proportion to the distance between the centers of the two charge distributions. The convergence of the excitation energies with respect to *N* are potentially problematic since the trial density matrices defined by Eq. (52), which are to be contracted with two-electron integrals, do not necessarily decay with increasing the unit cell index, unlike the regular ground-state density matrices that decay exponentially for insulators (see Ref. 33 and references therein).

The calculated excitation energies to the lowest singlet and triplet exciton states of polyethylene with different values of *N* are given in Tables I-IV. In these calculations, we hold *M* and *K* (the number of evenly spaced wave vector sampling points) fixed at 6 and 60, respectively. The total energies calculated by the ground-state HF and DFT methods converge up to 6 decimal places in hartree at *N*=4. The calculated band gaps are expected to show slower convergence than the total energies,<sup>70</sup> but they converge up to 3 decimal places in electron volts at *N*=6. It can be noticed from Table I that the CIS and TDHF excitation energies to the lowest singlet state show noticeably slower convergence with respect to *N* as compared with that of the total energies

TABLE I. Convergence of the total energy per  $C_2H_4$  unit ( $E$ ), band gap ( $E_g$ ), and vertical excitation energies to the lowest singlet and triplet exciton states with respect to the number of unit cells included in the lattice summations  $N$ . The HF, CIS, and TDHF calculations are carried out using the STO-3G basis set for an infinitely long all-*trans* polyethylene chain at the HF/STO-3G optimized geometry (CC bond length: 1.5451 Å; CH bond length: 1.0885 Å; CCC bond angle: 112.40 °; HCH bond angle: 107.07 °).

$N$	$K$	$E$ / hartree	$E_g$ / eV	CIS / eV		TDHF / eV	
				Singlet	Triplet	Singlet	Triplet
2	60	-77.160 404	23.697	15.715	14.123	15.668	12.968
4	60	-77.160 411	23.724	15.743	14.123	15.698	12.968
6	60	-77.160 411	23.725	15.753	14.123	15.706	12.968
10	60	-77.160 411	23.725	15.760	14.123	15.710	12.968
14	60	-77.160 411	23.725	15.761	14.123	15.712	12.968
18	60	-77.160 411	23.725	15.762	14.123	15.712	12.968
22	60	-77.160 411	23.725	15.763	14.123	15.713	12.968
26	60	-77.160 411	23.725	15.763	14.123	15.713	12.968
30	60	-77.160 411	23.725	15.763	14.123	15.713	12.968

or the band gaps. However, we can have these excitation energies converged up to 2 decimal places in electron volts at  $N=10$ , which is roughly twice as large a value of  $N$  as that required to obtain converged total energies and band gaps. For the TDDFT and TDDFT/TDA excitation energies, convergence can be achieved with a smaller value of  $N$  than that for the CIS and TDHF excitation energies. Therefore, it can be said that we can obtain the converged excitation energies by consistently taking into account only those two-electron integrals that are used in the preceding ground-state calculations and taking a slightly larger value of  $N$  than that for the total energy only calculations. We have observed that, although the trial density matrices for trial vectors do not necessarily decay with increasing the unit cell index, the corresponding density matrices for the converged solution vectors of the lowest transitions of polyethylene do decay exponentially. Tables I–IV also indicate that the excitation energies to the lowest triplet state are relatively insensitive to the choice of  $N$ .

In Tables V–VIII, we summarize the convergence of the calculated excitation energies with respect to  $K$  by holding  $M$  and  $N$  fixed at 6 and 14, respectively. It may be immediately

TABLE II. Convergence of the total energy per  $C_2H_4$  unit ( $E$ ), band gap ( $E_g$ ), and vertical excitation energies to the lowest singlet and triplet exciton states with respect to the number of unit cells included in the lattice summations  $N$ . The DFT, TDDFT, and TDDFT/TDA calculations using the SVWN functional and the STO-3G basis set are carried out for an infinitely long all-*trans* polyethylene chain at the geometry given in Table I.

$N$	$K$	$E$ / hartree	$E_g$ / eV	TDA / eV		TDDFT / eV	
				Singlet	Triplet	Singlet	Triplet
2	60	-76.948 043	12.185	12.187	12.165	12.187	12.164
4	60	-76.948 040	12.185	12.187	12.165	12.187	12.164
6	60	-76.948 039	12.185	12.188	12.165	12.188	12.164
10	60	-76.948 039	12.185	12.188	12.165	12.188	12.164
14	60	-76.948 039	12.185	12.188	12.165	12.188	12.164
18	60	-76.948 039	12.185	12.188	12.165	12.188	12.164
22	60	-76.948 039	12.185	12.188	12.165	12.188	12.164
26	60	-76.948 039	12.185	12.188	12.165	12.188	12.164
30	60	-76.948 039	12.185	12.188	12.165	12.188	12.164

TABLE III. Convergence of the total energy per  $C_2H_4$  unit ( $E$ ), band gap ( $E_g$ ), and vertical excitation energies to the lowest singlet and triplet exciton states with respect to the number of unit cells included in the lattice summations  $N$ . The DFT, TDDFT, and TDDFT/TDA calculations using the BLYP functional and the STO-3G basis set are carried out for an infinitely long all-*trans* polyethylene chain at the geometry given in Table I.

$N$	$K$	$E$ / hartree	$E_g$ / eV	TDA / eV		TDDFT / eV	
				Singlet	Triplet	Singlet	Triplet
2	60	-77.629 452	12.112	12.107	12.053	12.107	12.046
4	60	-77.629 451	12.111	12.109	12.052	12.109	12.046
6	60	-77.629 451	12.111	12.109	12.052	12.109	12.046
10	60	-77.629 451	12.111	12.110	12.052	12.110	12.046
14	60	-77.629 451	12.111	12.110	12.052	12.110	12.046
18	60	-77.629 451	12.111	12.110	12.052	12.110	12.046
22	60	-77.629 451	12.111	12.110	12.052	12.110	12.046
26	60	-77.629 451	12.111	12.110	12.052	12.110	12.046
30	60	-77.629 451	12.111	12.110	12.052	12.110	12.046

noticed that the calculated total energies and band gaps are converged up to the decimal places given in the tables at  $K=20$  and they do not change as  $K$  increases. The calculated CIS and TDHF excitation energies are also insensitive to the choice of  $K$  as long as  $K \geq 20$  (Table V). In contrast to this, the TDDFT and TDDFT/TDA excitation energies undergo noticeable changes upon increasing  $K$ ; they do not converge up to 3 decimal places in electron volts until  $K$  becomes as large as 80, although for practical purposes the excitation energies obtained with  $K=20$  seem sufficiently close to the converged results. It is interesting to note that the SVWN and BLYP excitation energies to the lowest singlet exciton states approach the corresponding KS band gaps. Among the calculated excitation energies to triplet states also, there are those states whose excitation energies approach the corresponding KS band gaps. These results persist in the calculations using larger basis sets (vide post) and those for other polymeric systems, and are not coincidental.

As we have noted previously,<sup>36</sup> the excited-state wave functions obtained from the TDDFT and TDDFT/TDA calculations are very often dominated by only one singly excited configuration, unlike those of CIS and TDHF which are generally linear combinations of a number of those configura-

TABLE IV. Convergence of the total energy per  $C_2H_4$  unit ( $E$ ), band gap ( $E_g$ ), and vertical excitation energies to the lowest singlet and triplet exciton states with respect to the number of unit cells included in the lattice summations  $N$ . The DFT, TDDFT, and TDDFT/TDA calculations using the B3LYP functional and the STO-3G basis set are carried out for an infinitely long all-*trans* polyethylene chain at the geometry given in Table I.

$N$	$K$	$E$ / hartree	$E_g$ / eV	TDA / eV		TDDFT / eV	
				Singlet	Triplet	Singlet	Triplet
2	60	-77.636 780	14.410	13.465	13.176	13.459	13.147
4	60	-77.636 782	14.417	13.443	13.145	13.442	13.117
6	60	-77.636 782	14.417	13.441	13.141	13.440	13.114
10	60	-77.636 782	14.418	13.443	13.141	13.442	13.114
14	60	-77.636 782	14.418	13.444	13.141	13.443	13.114
18	60	-77.636 782	14.418	13.444	13.141	13.443	13.114
22	60	-77.636 782	14.418	13.445	13.141	13.443	13.114
26	60	-77.636 782	14.418	13.445	13.141	13.444	13.114
30	60	-77.636 782	14.418	13.445	13.141	13.444	13.114

TABLE V. Convergence of the total energy per  $C_2H_4$  unit ( $E$ ), band gap ( $E_g$ ), and vertical excitation energies to the lowest singlet and triplet exciton states with respect to the number of wave vector sampling points  $K$ . The HF, CIS, and TDHF calculations are carried out using the STO-3G basis set for an infinitely long all-*trans* polyethylene chain at the geometry given in Table I.

$N$	$K$	$E$ / hartree	$E_g$ / eV	CIS / eV		TDHF / eV	
				Singlet	Triplet	Singlet	Triplet
14	20	-77.160 411	23.725	15.761	14.123	15.712	12.968
14	40	-77.160 411	23.725	15.761	14.123	15.712	12.968
14	60	-77.160 411	23.725	15.761	14.123	15.712	12.968
14	80	-77.160 411	23.725	15.761	14.123	15.712	12.968
14	100	-77.160 411	23.725	15.761	14.123	15.712	12.968

rations. In our example, the TDDFT and TDDFT/TDA excited-state wave functions of the lowest singlet exciton states of polyethylene are dominated by the configuration in which an electron is promoted from the highest valence band at the Brillouin zone center to the lowest conduction band at the same position in the Brillouin zone. In the corresponding CIS and TDHF excited-state wave functions, on the other hand, the contributions from the configurations having different wave vectors are mixed. It should be noted that the weight of each singly excited configuration in the CIS and TDHF wave functions exhibits correct scaling with respect to  $K$ ; as  $K$  increases, the weight decreases in proportion to  $K^{-1/2}$  such that the sum of the squared weights equal to unity and the overall shape of wave functions remains unchanged. However, the TDDFT and TDDFT/TDA wave functions do not have this correct scaling properties, and they are more and more dominated by a single configuration as  $K$  increases. This means that the TDDFT and TDDFT/TDA excitation energies to the lowest singlet exciton states of polyethylene approach the diagonal elements of the  $\mathbf{A}$  matrix in the limit of  $K \rightarrow \infty$ . Since the diagonal elements of the  $\mathbf{A}$  matrix is a sum of the KS orbital energy difference ( $\epsilon_{a\sigma}^{[k_i]} - \epsilon_{i\sigma}^{[k_i]}$ ) and two-electron integrals and the latter quantities are proportional to  $K^{-1}$ , one of the TDDFT and TDDFT/TDA excitation energies collapses to the KS band gap in the limit of  $K \rightarrow \infty$ .

From the viewpoint of the matrix elements, the slow convergence of the TDDFT and TDDFT/TDA excitation energies with respect to  $K$  is a consequence of the fact that the

TABLE VI. Convergence of the total energy per  $C_2H_4$  unit ( $E$ ), band gap ( $E_g$ ), and vertical excitation energies to the lowest singlet and triplet exciton states with respect to the number of wave vector sampling points  $K$ . The DFT, TDDFT, and TDDFT/TDA calculations using the SVWN functional and the STO-3G basis set are carried out for an infinitely long all-*trans* polyethylene chain at the geometry given in Table I.

$N$	$K$	$E$ / hartree	$E_g$ / eV	TDA / eV		TDDFT / eV	
				Singlet	Triplet	Singlet	Triplet
14	20	-76.948 039	12.185	12.195	12.149	12.195	12.148
14	40	-76.948 039	12.185	12.190	12.162	12.190	12.161
14	60	-76.948 039	12.185	12.188	12.165	12.188	12.164
14	80	-76.948 039	12.185	12.187	12.166	12.187	12.165
14	100	-76.948 039	12.185	12.186	12.166	12.186	12.165

TABLE VII. Convergence of the total energy per  $C_2H_4$  unit ( $E$ ), band gap ( $E_g$ ), and vertical excitation energies to the lowest singlet and triplet exciton states with respect to the number of wave vector sampling points  $K$ . The DFT, TDDFT, and TDDFT/TDA calculations using the BLYP functional and the STO-3G basis set are carried out for an infinitely long all-*trans* polyethylene chain at the geometry given in Table I.

$N$	$K$	$E$ / hartree	$E_g$ / eV	TDA / eV		TDDFT / eV	
				Singlet	Triplet	Singlet	Triplet
14	20	-77.629 451	12.111	12.106	12.034	12.106	12.028
14	40	-77.629 451	12.111	12.109	12.050	12.109	12.045
14	60	-77.629 451	12.111	12.110	12.052	12.110	12.046
14	80	-77.629 451	12.111	12.110	12.053	12.110	12.046
14	100	-77.629 451	12.111	12.110	12.053	12.110	12.046

two-electron integrals of the type  $(ab|ji)$  are replaced by the exchange-correlation integrals of the type  $(ai|w|jb)$  in Eqs. (33) and (34) on going from TDHF (CIS) to TDDFT (TDDFT/TDA). These two-electron integrals are supposed to cancel spurious self-interaction energies in the orbital energies  $\epsilon$  (see Ref. 71). However, while the interaction between the two charge distributions in the former integrals  $(ab|ji)$  is Coulomb type, which may decay in inverse proportion to the distance between these two charge distributions, the latter integrals  $(ai|w|jb)$  decay exponentially due to the particular form of the current approximate functionals. While in the CIS and TDHF calculations, the self-interaction energies in  $\epsilon$  are properly cancelled by the two-electron integrals  $(ab|ji)$ , in the TDDFT calculations, the cancellation is incomplete because of the too rapid decay of the integrals  $(ai|w|jb)$ . Since parameter  $K$  physically corresponds to the size of the system,<sup>72</sup> we can regard the slow convergence of the TDDFT and TDDFT/TDA excitation energies with respect to  $K$  as being due to the fact that the contribution of the integrals  $(ai|w|jb)$  become disproportionately small relative to that of  $\epsilon$  as  $K$  becomes large. The observation that the TDDFT and TDDFT/TDA excitation energies to the lowest singlet exciton states tend to collapse to the KS band gaps and that the associated wave functions do not exhibit correct scaling behavior with increasing  $K$  is likewise accounted for by the incomplete cancellation of the self-interaction energies (see also the discussions given by Perdew and co-workers<sup>73-75</sup>).

Obviously, the above-mentioned problems in the TD-DFT and TDDFT/TDA excitation energies are closely re-

TABLE VIII. Convergence of the total energy per  $C_2H_4$  unit ( $E$ ), band gap ( $E_g$ ), and vertical excitation energies to the lowest singlet and triplet exciton states with respect to the number of wave vector sampling points  $K$ . The DFT, TDDFT, and TDDFT/TDA calculations using the B3LYP functional and the STO-3G basis set are carried out for an infinitely long all-*trans* polyethylene chain at the geometry given in Table I.

$N$	$K$	$E$ / hartree	$E_g$ / eV	TDA / eV		TDDFT / eV	
				Singlet	Triplet	Singlet	Triplet
14	20	-77.636 782	14.418	13.443	13.141	13.442	13.113
14	40	-77.636 782	14.418	13.444	13.141	13.443	13.114
14	60	-77.636 782	14.418	13.444	13.141	13.443	13.114
14	80	-77.636 782	14.418	13.444	13.141	13.443	13.114
14	100	-77.636 782	14.418	13.444	13.141	13.443	13.114

TABLE IX. Convergence of the total energy per  $C_2H_4$  unit ( $E$ ), HOMO–LUMO energy difference ( $E_g$ ), and vertical excitation energies to the lowest singlet and triplet excited states of all-*trans*  $n$ -alkane  $H(CH_2)_nH$  molecules with respect to the chain length  $n$ . The HF, CIS, and TDHF calculations are carried out using the STO-3G basis set at the geometry given in Table I.

$n$	$E$ / hartree	$E_g$ / eV	CIS / eV		TDHF / eV	
			Singlet	Triplet	Singlet	Triplet
5	−77.618 442	26.7	17.685	14.414	17.666	13.293
10	−77.389 427	25.0	16.542	14.203	16.516	13.063
20	−77.274 919	24.1	16.041	14.143	16.004	12.994
40	−77.217 665	23.9	15.855	14.128	15.811	12.976
$\infty^a$	−77.160 411	23.725	15.763	14.123	15.713	12.968

<sup>a</sup>Crystalline orbital calculations with  $N=30$  and  $K=60$ .

lated to the well-known common flaw that many of the current approximate functionals share; the exchange potentials generated from these functionals decay too rapidly in the asymptotic region.<sup>54,76,77</sup> In the TDDFT calculations on molecules, serious numerical errors manifest themselves as the excitation energies approach the negative of the highest occupied KS orbital energies,<sup>76</sup> which are typically significantly higher than the excitation energies of the several lowest singlet or triplet excited states. For extended systems, the effects of this flaw seem to be more acute since the negative of the highest occupied KS orbital energies may often be lower than the excitation energies to the lowest exciton states (for example, the highest occupied KS orbital energies of polyethylene are at −4.9, −4.9, and −6.1 eV, respectively, at the SVWN/STO-3G, BLYP/STO-3G, and B3LYP/STO-3G levels). These results suggest that considerable caution must be given to the calculated TDDFT and TDDFT/TDA excitation energies of extended systems when they are compared with the experimental data.

Tables IX–XII compare the calculated excitation energies of  $n$ -alkane molecules containing 5, 10, 20, and 40 carbon atoms with those of an infinitely long polyethylene chain. Due to the terminal groups of the oligomers, whose effects decay roughly in inverse proportion to the chain length  $n$ , the calculated quantities of  $n$ -alkane molecules exhibit very slow convergence with respect to  $n$ , although they smoothly approach the limiting values of the infinite chain predicted by the crystalline orbital calculations as  $n$  increases

TABLE X. Convergence of the total energy per  $C_2H_4$  unit ( $E$ ), HOMO–LUMO energy difference ( $E_g$ ), and vertical excitation energies to the lowest singlet and triplet excited states of all-*trans*  $n$ -alkane  $H(CH_2)_nH$  molecules with respect to the chain length  $n$ . The DFT, TDDFT, and TDDFT/TDA calculations using the SVWN functional and the STO-3G basis set are carried out at the geometry given in Table I.

$n$	$E$ / hartree	$E_g$ / eV	TDA / eV		TDDFT / eV	
			Singlet	Triplet	Singlet	Triplet
5	−77.404 006	14.5	14.894	14.093	14.889	14.005
10	−77.176 009	13.1	13.393	12.964	13.382	12.960
20	−77.062012	12.5	12.592	12.413	12.592	12.412
40	−77.005 014	12.3	12.305	12.228	12.305	12.227
$\infty^a$	−76.948 039	12.185	12.188	12.165	12.188	12.164

<sup>a</sup>Crystalline orbital calculations with  $N=30$  and  $K=60$ .

TABLE XI. Convergence of the total energy per  $C_2H_4$  unit ( $E$ ), HOMO–LUMO energy difference ( $E_g$ ), and vertical excitation energies to the lowest singlet and triplet excited states of all-*trans*  $n$ -alkane  $H(CH_2)_nH$  molecules with respect to the chain length  $n$ . The DFT, TDDFT, and TDDFT/TDA calculations using the BLYP functional and the STO-3G basis set are carried out at the geometry given in Table I.

$n$	$E$ / hartree	$E_g$ / eV	TDA / eV		TDDFT / eV	
			Singlet	Triplet	Singlet	Triplet
5	−78.100 733	14.4	14.852	13.802	14.835	13.622
10	−77.865 080	13.0	13.268	12.763	13.258	12.749
20	−77.747 256	12.4	12.485	12.259	12.485	12.250
40	−77.688 344	12.2	12.213	12.100	12.213	12.098
$\infty^a$	−77.629 451	12.111	12.110	12.052	12.110	12.046

<sup>a</sup>Crystalline orbital calculations with  $N=30$  and  $K=60$ .

(Fig. 1). Insofar as the total energies are concerned, we can eliminate the effects of terminal groups by taking the energy difference of two  $n$ -alkane molecules with different chain lengths. Since total energies are size-extensive quantities, such a treatment can be justified and the resulting energy differences converge reasonably rapidly with increasing  $n$ . However, it is difficult to think of a similar extrapolation scheme for excitation energies and band gaps. These tables indicate that the calculated excitation energies and band gaps do not converge up to one decimal place in electron volts even at  $n=40$ . Considering that these quantities of an infinitely long polyethylene chain converge up to 2 decimal places in electron volts at  $N=14$  (vide ante), the single-excitation theories based on crystalline orbital theory constitute a distinct advantage over the oligomer extrapolation approach. In other words, the periodic boundary conditions are particularly suited for the calculations of excitation energies and band gaps of infinitely extended systems. This conclusion, however, does not deny the practical usefulness of the oligomer extrapolation approach. The oligomer extrapolation approach is in many cases complementary to the crystalline orbital theory approach, since it provides important information about the convergence behavior of the properties of oligomers and one can check the soundness of both the approaches by comparing the properties of infinitely extended systems obtained from them. It should also be noted that the TDDFT and TDDFT/TDA excitation energies to the lowest

TABLE XII. Convergence of the total energy per  $C_2H_4$  unit ( $E$ ), HOMO–LUMO energy difference ( $E_g$ ), and vertical excitation energies to the lowest singlet and triplet excited states of all-*trans*  $n$ -alkane  $H(CH_2)_nH$  molecules with respect to the chain length  $n$ . The DFT, TDDFT, and TDDFT/TDA calculations using the B3LYP functional and the STO-3G basis set are carried out at the geometry given in Table I.

$n$	$E$ / hartree	$E_g$ / eV	TDA / eV		TDDFT / eV	
			Singlet	Triplet	Singlet	Triplet
5	−78.109 761	16.8	15.614	14.275	15.598	13.995
10	−77.873 262	15.4	14.279	13.584	14.270	13.551
20	−77.755 013	14.7	13.697	13.251	13.694	13.225
40	−77.695 890	14.5	13.517	13.167	13.517	13.143
$\infty^a$	−77.636 782	14.418	13.445	13.141	13.444	13.114

<sup>a</sup>Crystalline orbital calculations with  $N=30$  and  $K=60$ .

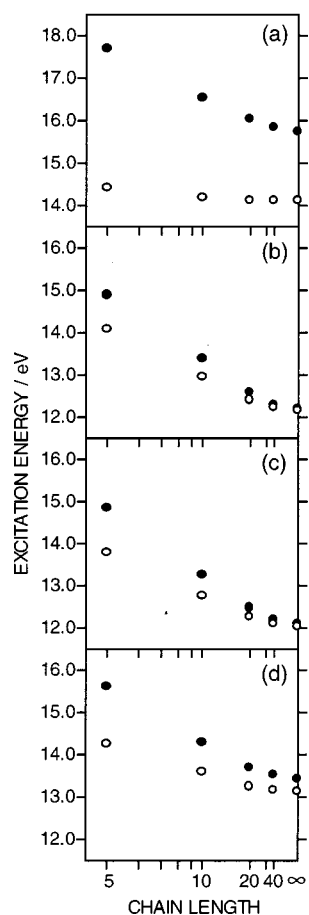


FIG. 1. The vertical excitation energies to the lowest singlet (filled circles) and triplet (open circles) excited states of all-*trans*  $n$ -alkane  $\text{H}(\text{CH}_2)_n\text{H}$  molecules and of an infinitely long all-*trans* polyethylene chain as a function of the chain length  $n$ . The theoretical models employed are the (a) CIS/STO-3G and the TDDFT methods at the (b) SVWN/STO-3G, (c) BLYP/STO-3G, and (d) B3LYP/STO-3G levels.

singlet states of  $n$ -alkane molecules rapidly approach the corresponding HOMO–LUMO orbital energy differences as  $n$  becomes larger, which is consistent with the results of the crystalline orbital calculations.

In Table XIII, we summarize the excitation energies to the lowest singlet exciton state calculated by using five different basis sets ranging from STO-3G to 6-31G\*\* (containing Cartesian 6d functions). The geometry used is the one optimized at the B3LYP/6-31G\* level and is in good agreement with the experimental data obtained from x-ray diffraction studies.<sup>78</sup> We observe that the Tamm–Dancoff approximation introduces practically negligible errors in the calculated TDDFT excitation energies, as we noted in our previous study on molecules.<sup>36</sup> Since in the crystalline orbital calculations using complex orbitals we cannot bring the TDDFT matrix eigenvalue equation to one of half the dimension, the Tamm–Dancoff approximation reduces the cpu time usage roughly by a factor of two without changing the calculated results significantly.

We expect that the basis-set dependence will be greater on the excited-state properties that involve the virtual orbitals than the ground-state properties that are primarily determined by the occupied orbitals. Insofar as the lowest singlet

TABLE XIII. The total energies ( $E$ ), negatives of the highest occupied orbital energies ( $-\epsilon$ ), band gaps ( $E_g$ ), and vertical excitation energies to the lowest singlet exciton state of an infinitely long all-*trans* polyethylene chain at the B3LYP/6-31G\* optimized geometry (CC bond length: 1.5344 Å; CH bond length: 1.1005 Å; CCC bond angle: 113.60°; HCH bond angle: 105.94°).

Theory	$E$ / hartree	$-\epsilon$ / eV	$E_g$ / eV	TDA <sup>a</sup> / eV	TDDFT <sup>b</sup> / eV
HF/STO-3G	-77.159 644	9.72	23.80	15.89	15.84
HF/3-21G	-77.637 596	10.85	17.85	12.53	12.51
HF/6-31G	-78.036 449	10.84	16.88	11.70	11.68
HF/6-31G*	-78.068 975	10.92	17.02	11.77	11.75
HF/6-31G**	-78.075 058	10.90	17.00	11.75	...
SVWN/STO-3G	-76.948 513	5.09	12.25	12.25	12.25
SVWN/3-21G	-77.462 437	6.66	8.81	8.82	8.82
SVWN/6-31G	-77.862 181	6.58	8.07	8.08	8.08
SVWN/6-31G*	-77.881 935	6.51	8.01	8.01	8.01
SVWN/6-31G**	-77.886 817	6.55	8.03	8.03	...
BLYP/STO-3G	-77.629 772	5.15	12.18	12.18	12.18
BLYP/3-21G	-78.146 333	6.36	8.81	8.82	8.82
BLYP/6-31G	-78.554 066	6.27	8.09	8.09	8.09
BLYP/6-31G*	-78.571 183	6.20	8.03	8.04	8.04
BLYP/6-31G**	-78.576 883	6.24	8.06	8.06	...
B3LYP/STO-3G	-77.636 834	6.30	14.49	13.52	13.52
B3LYP/3-21G	-78.144 078	7.51	10.67	9.95	9.94
B3LYP/6-31G	-78.549 646	7.43	9.90	9.19	9.18
B3LYP/6-31G*	-78.568 977	7.36	9.86	9.14	9.14
B3LYP/6-31G**	-78.574 563	7.39	9.88	9.16	...
Experiment <sup>c</sup>	...	8.8	...	7.6	7.6

<sup>a</sup>CIS or TDDFT/TDA calculations with  $N=14$  and  $K=60$ .

<sup>b</sup>TDHF or TDDFT calculations with  $N=14$  and  $K=60$ .

<sup>c</sup>References 1 and 3.

exciton state of polyethylene is concerned, however, the calculated excitation energies show reasonably rapid convergence with respect to the basis set size. The present results, nevertheless, do not rule out possible important roles of diffuse basis functions. Experimentally, the optical absorption band edge of polyethylene is located at around 7.6 eV, which is substantially lower than the threshold of photoemission (8.8 eV).<sup>1,3</sup> We compare the latter experimental data with the first ionization potential of polyethylene, i.e., the negatives of the highest occupied orbital energies. Approximating the ionization potential by the negatives of the highest occupied orbital energies is justified by the Koopmans' theorem for the HF calculations and by the theorem proven by Levy, Perdew, and Sahni<sup>79</sup> and by Almbladh and von Barth<sup>80</sup> for the DFT calculations. It should be noted that the previous experimental studies (Ref. 5 and references therein) interpreted the threshold of photoconduction as corresponding to the fundamental band gap. In this paper, we confine our discussions to the optical absorption band edge and the threshold of photoemission. The theoretical interpretation of the threshold of photoconduction will be discussed in our forthcoming paper.<sup>81</sup>

The CIS and TDHF methods yield the excitation energies to the lowest singlet exciton states that are substantially lower than the band gaps, and are significantly closer to the measured optical absorption band edge than the band gaps. This result substantiates our expectation that the CIS and TDHF methods describe more appropriately the optical absorption process than does the simple band-to-band transition picture. Quantitatively, however, the calculated CIS and

TDHF excitation energies are significantly higher than the experimental values. We consider that the CIS and TDHF description of the exciton states to be a zeroth-order description, on the basis of which we can incorporate the electron correlation effects systematically. The negatives of the highest occupied orbital energies obtained from the ground-state HF calculations overestimate the measured photoemission threshold by a few electron volts. The HF theory and HF-based single-excitation theories (CIS and TDHF) fail to reproduce the correct ordering of the optical absorption band edge and the photoemission threshold. Sun and Bartlett<sup>82</sup> have shown that a large proportion of the error in the ionization potential of polyethylene could be eliminated by incorporating the electron correlation effects via second-order many-body perturbation theory. We expect that the inclusion of electron correlation in the same model would lead to a significant improvement in the excitation energies.

The TDDFT and TDDFT/TDA methods yield the excitation energies to the lowest singlet exciton state, which are in fair agreement with the experimentally measured position of the optical absorption band edge. As we have observed in the STO-3G calculation results, these excitation energies are practically the same as the corresponding KS band gaps even for basis sets larger than the STO-3G. As one might anticipate,<sup>54,76,77</sup> the negatives of the highest occupied KS orbital energies underestimate the experimental values by a few electron volts. This is due to the too rapid decay of the approximate exchange potentials generated from the current approximate exchange–correlation functionals. As a consequence, the TDDFT and TDDFT/TDA methods also fail to reproduce the correct ordering of the optical absorption band edge and the photoemission threshold, although the origin of the failure is different from that of the HF and HF-based single-excitation theories. Despite the agreement between the TDDFT excitation energies and the experimental data, it seems too hasty to conclude that the TDDFT and TDDFT/TDA methods are superior to the CIS and TDHF methods for extended systems, for the following two reasons. First, the wave functions obtained from the TDDFT calculations do not show correct scaling with increasing  $K$  due to the incomplete cancellation of self-interaction energies. We expect the wave functions to keep their shape unchanged as  $K$  increases if  $K$  is sufficiently large. Second, the calculated excitation energies to the lowest singlet exciton states fall higher than the negative of the highest occupied KS orbital energy. It has been shown that substantial errors manifest themselves as the excitation energies approach this threshold energy, and the excitation energies above this threshold are not reliable, when the current approximate functionals are used.<sup>76</sup>

The HF/DFT hybrid functional provides calculated results which are in between those obtained from the HF-based single-excitation theories and those of TDDFT using the pure exchange–correlation functionals. Consequently, the ionization potentials and the excitation energies are significantly closer to the experimental data than are the Koopmans' ionization potential and the CIS and TDHF excitation energies, respectively. However, these numbers are obviously strongly dependent on the mixing ratio of the HF ex-

change in the hybrid functional, and the choice of the mixing ratio seems too arbitrary for the purpose of calculating the excitation energies.

## V. CONCLUSION

In this article, we present the general formalism for time-dependent linear response theory for extended systems within the framework of LCAO crystalline orbital theory, which encompasses the formalisms of TDHF, CIS, TDDFT, and TDDFT/TDA as particular cases. These single-excitation theories are implemented in an efficient direct algorithm that employs trial-vector techniques to avoid the explicit formation of two-electron integrals over the crystalline-orbital basis. The methods are applied to polyethylene to study the dependence of the calculated excitation energies on the several parameters of the calculations and to compare the calculated excitation energies against the experimental data. The important results are summarized as follows.

First, the CIS and TDHF excitation energies exhibit noticeably slower convergence with respect to  $N$  than the total energies and band gaps calculated at the same theoretical model. However, we can obtain converged excitation energies with respect to  $N$  by taking roughly twice as large a value of  $N$  as that required to obtain the converged total energies and band gaps. The CIS and TDHF excitation energies show, on the other hand, very rapid convergence with respect to  $K$ . The CIS and TDHF excitation energies and wave functions obtained in this way might be considered as appropriate zeroth-order descriptions of optical absorption processes of many polymers, which are much more realistic than the simple band-to-band transition pictures. Quantitatively, however, these calculated excitation energies are significantly overestimated, the errors being as large as a few electron volts.

Second, we find that the TDDFT and TDDFT/TDA excitation energies exhibit slow convergence with respect to  $K$ . Although, for practical purposes, the calculated excitation energies obtained with a reasonably small value of  $K$  would have sufficient numerical precision (as compared to the converged values), this result indicates that the TDDFT and TDDFT/TDA methods employing current approximate functionals may no longer be a theoretically sound procedure when they are applied to extended systems within the framework of crystalline orbital theory. We consider that the slow convergence is a consequence of the incomplete cancellation of the self-interaction energies and is closely connected to the well-known too rapid decay of the exchange–correlation potentials generated from the current approximate exchange–correlation functionals.

None of the methods studied here correctly reproduce the experimental findings that the optical absorption band edge of polyethylene, i.e., the excitation energy to the lowest singlet exciton state, occurs lower than the threshold of photoemission, which corresponds to the first ionization potential. The most promising direction of future research to overcome this failure will be to incorporate the electron correlation effects in the calculated excitation energies obtained from the HF-based single-excitation theories.<sup>81</sup> Another possible solution is to employ a theoretically more rig-

orous exchange functional, which does not introduce self-interaction errors, in the TDDFT and TDDFT/TDA calculations. The exact multiplicative exchange potential method, which has recently been implemented within the LCAO KS framework,<sup>83</sup> will be one such functional.

## ACKNOWLEDGMENTS

Illuminating discussions with Dr. Stanislav Ivanov and Dr. Jun-Qiang Sun, Quantum Theory Project, University of Florida, are greatly appreciated. This work was supported by U.S. Air Force Office of Scientific Research under Grant No. F49620-98-0116.

- <sup>1</sup>R. A. George, D. H. Martin, and E. G. Wilson, *J. Phys. C* **5**, 871 (1972).
- <sup>2</sup>M. Fujihira and H. Inokuchi, *Chem. Phys. Lett.* **17**, 554 (1972).
- <sup>3</sup>K. J. Less and E. G. Wilson, *J. Phys. C* **6**, 3110 (1973).
- <sup>4</sup>J. Delhalle *et al.*, *J. Chem. Phys.* **60**, 595 (1974).
- <sup>5</sup>D. Bloor *et al.*, *Chem. Phys. Lett.* **40**, 323 (1976).
- <sup>6</sup>G. Wegner, *Makromol. Chem.* **154**, 35 (1972).
- <sup>7</sup>D. Bloor, *J. Mater. Sci.* **10**, 1678 (1975).
- <sup>8</sup>D. Bloor, G. C. Stevens, P. J. Page, and P. M. Williams, *Chem. Phys. Lett.* **33**, 61 (1975).
- <sup>9</sup>S. Suhai, in *Quantum Chemistry of Polymers—Solid State Aspects*, edited by J. Ladik, J.-M. André, and M. Seel (Reidel, Braunschweig, 1983).
- <sup>10</sup>S. Suhai, *Phys. Rev. B* **29**, 4570 (1984).
- <sup>11</sup>S. Suhai, *Int. J. Quantum Chem., Quantum Chem. Symp.* **18**, 161 (1984).
- <sup>12</sup>S. Suhai, *Int. J. Quantum Chem.* **29**, 469 (1986).
- <sup>13</sup>S. Suhai, *J. Chem. Phys.* **85**, 611 (1986).
- <sup>14</sup>M. Rohlfing and S. G. Louie, *Phys. Rev. Lett.* **80**, 3320 (1998).
- <sup>15</sup>M. Rohlfing and S. G. Louie, *Phys. Rev. Lett.* **81**, 2312 (1998).
- <sup>16</sup>M. Rohlfing and S. G. Louie, *Phys. Rev. Lett.* **82**, 1959 (1999).
- <sup>17</sup>M. G. Vracko and M. Zaidler, *Int. J. Quantum Chem.* **43**, 321 (1992).
- <sup>18</sup>M. G. Vracko and M. Zaidler, *Int. J. Quantum Chem.* **47**, 119 (1993).
- <sup>19</sup>M. Vracko, B. Champagne, D. H. Mosley, and J.-M. André, *J. Chem. Phys.* **102**, 6831 (1995).
- <sup>20</sup>A. L. Fetter and J. D. Walecka, *Quantum Theory of Many-Particle Systems* (McGraw-Hill, New York, 1971).
- <sup>21</sup>C.-M. Liegener and J. Ladik, *Phys. Rev. B* **35**, 6403 (1987).
- <sup>22</sup>M. Vracko, C.-M. Liegener, and J. Ladik, *Int. J. Quantum Chem.* **37**, 241 (1990).
- <sup>23</sup>B. Champagne, J. G. Fripiat, and J.-M. André, *J. Chem. Phys.* **96**, 8330 (1992).
- <sup>24</sup>B. Champagne, D. H. Mosley, J. G. Fripiat, and J.-M. André, *Int. J. Quantum Chem.* **46**, 1 (1993).
- <sup>25</sup>B. Champagne, J.-M. André, and Y. Öhrn, *Int. J. Quantum Chem.* **57**, 811 (1996).
- <sup>26</sup>P. Otto, F. L. Gu, and J. Ladik, *J. Chem. Phys.* **110**, 2717 (1999).
- <sup>27</sup>E. Runge and E. K. U. Gross, *Phys. Rev. Lett.* **52**, 997 (1984).
- <sup>28</sup>E. K. U. Gross and W. Kohn, *Adv. Quantum Chem.* **21**, 255 (1990).
- <sup>29</sup>M. Petersilka, U. J. Gossmann, and E. K. U. Gross, *Phys. Rev. Lett.* **76**, 1212 (1996).
- <sup>30</sup>M. E. Casida, in *Recent Advances in Density Functional Methods, Part I*, edited by D. P. Chong (World Scientific, Singapore, 1995).
- <sup>31</sup>G. Del Re, J. Ladik, and G. Biczó, *Phys. Rev.* **155**, 997 (1967).
- <sup>32</sup>J. M. André, *J. Chem. Phys.* **50**, 1536 (1969).
- <sup>33</sup>M. Kertész, *Adv. Quantum Chem.* **15**, 161 (1982).
- <sup>34</sup>J. J. Ladik, *Quantum Theory of Polymers as Solids* (Plenum, New York, 1988).
- <sup>35</sup>J.-Q. Sun and R. J. Bartlett, *Topics in Current Chemistry* (Springer-Verlag, Berlin, 1999), Vol. 203.
- <sup>36</sup>S. Hirata and M. Head-Gordon, *Chem. Phys. Lett.* (in press).
- <sup>37</sup>E. R. Davidson, *J. Comput. Phys.* **17**, 87 (1975).
- <sup>38</sup>J. Olsen, H. J. Aa. Jensen, and P. Jørgensen, *J. Comput. Phys.* **74**, 265 (1988).
- <sup>39</sup>J. B. Foresman, M. Head-Gordon, J. A. Pople, and M. J. Frisch, *J. Phys. Chem.* **96**, 135 (1992).
- <sup>40</sup>H. Weiss, R. Ahlrichs, and M. Häser, *J. Chem. Phys.* **99**, 1262 (1993).
- <sup>41</sup>R. Bauernschmitt, M. Häser, O. Treutler, and R. Ahlrichs, *Chem. Phys. Lett.* **264**, 573 (1997).
- <sup>42</sup>J. Almlöf, K. Faegri, Jr., and K. Korsell, *J. Comput. Chem.* **3**, 385 (1982).
- <sup>43</sup>R. McWeeny, *Methods of Molecular Quantum Mechanics*, 2nd ed. (Academic, San Diego, 1992).
- <sup>44</sup>S. Suhai, *Phys. Rev. B* **51**, 16553 (1995).
- <sup>45</sup>S. Hirata and S. Iwata, *J. Chem. Phys.* **107**, 10075 (1997).
- <sup>46</sup>S. Hirata and S. Iwata, *J. Phys. Chem. A* **102**, 8426 (1998).
- <sup>47</sup>J. A. Pople, P. M. W. Gill, and B. G. Johnson, *Chem. Phys. Lett.* **199**, 557 (1992).
- <sup>48</sup>B. G. Johnson, P. M. W. Gill, and J. A. Pople, *J. Chem. Phys.* **98**, 5612 (1993).
- <sup>49</sup>R. Bauernschmitt and R. Ahlrichs, *Chem. Phys. Lett.* **256**, 454 (1996).
- <sup>50</sup>S. Hirata and M. Head-Gordon, *Chem. Phys. Lett.* **302**, 375 (1999).
- <sup>51</sup>R. J. Bartlett and E. J. Brändas, *J. Chem. Phys.* **56**, 5467 (1972).
- <sup>52</sup>R. J. Bartlett and E. J. Brändas, *J. Chem. Phys.* **59**, 2032 (1973).
- <sup>53</sup>K. Hirao and H. Nakatsuji, *J. Comput. Phys.* **45**, 246 (1982).
- <sup>54</sup>C. Jamorski, M. E. Casida, and D. R. Salahub, *J. Chem. Phys.* **104**, 5134 (1996).
- <sup>55</sup>R. E. Stratmann, G. E. Scuseria, and M. J. Frisch, *J. Chem. Phys.* **109**, 8218 (1998).
- <sup>56</sup>R. Bauernschmitt and R. Ahlrichs, *J. Chem. Phys.* **104**, 9047 (1996).
- <sup>57</sup>POLYMER Version 1.0 is a crystalline orbital program package for infinite one-dimensional lattices written by S. Hirata in collaboration with M. Tasumi, H. Torii, S. Iwata, M. Head-Gordon, and R. J. Bartlett. The available theoretical methods include Hartree-Fock theory (total energies, energy bands, and analytical energy gradients), second-order many-body perturbation theory (total energies and quasiparticle energy bands), many-body Green's function theory (quasiparticle energy bands), density functional theory (local, gradient-corrected, and hybrid functionals, total energies, energy bands, and analytical energy gradients), and single-excitation theories (configuration interaction singles, time-dependent Hartree-Fock, and time-dependent density functional theory) (unpublished).
- <sup>58</sup>S. Hirata and S. Iwata, *J. Chem. Phys.* **108**, 7901 (1998).
- <sup>59</sup>S. Hirata, H. Torii, and M. Tasumi, *Phys. Rev. B* **57**, 11994 (1998).
- <sup>60</sup>S. Hirata and S. Iwata, *J. Mol. Struct.: THEOCHEM* **451**, 121 (1998).
- <sup>61</sup>S. Hirata and S. Iwata, *J. Chem. Phys.* **109**, 4147 (1998).
- <sup>62</sup>J. C. Slater, *Quantum Theory of Molecules and Solids, Vol. 4: The Self-Consistent Field for Molecules and Solids* (McGraw-Hill, New York, 1974).
- <sup>63</sup>S. H. Vosko, L. Wilk, and M. Nusair, *Can. J. Phys.* **58**, 1200 (1980), Parameterization 5.
- <sup>64</sup>A. D. Becke, *Phys. Rev. A* **38**, 3098 (1988).
- <sup>65</sup>C. Lee, W. Yang, and R. G. Parr, *Phys. Rev. B* **37**, 785 (1988).
- <sup>66</sup>A. D. Becke, *J. Chem. Phys.* **98**, 5648 (1993).
- <sup>67</sup>C. A. White, J. Kong, D. R. Maurice, T. R. Adams, J. Baker, M. Challacombe, E. Schwegler, J. P. Dombroski, C. Ochsenfeld, M. Oumi, T. R. Furlani, J. Florian, R. D. Adamson, N. Nair, A. M. Lee, N. Ishikawa, R. L. Graham, A. Warshel, B. G. Johnson, P. M. W. Gill, and M. Head-Gordon, Q-CHEM. Version 1.2, Q-Chem, Inc., Pittsburgh, PA (1998).
- <sup>68</sup>H. Teramae, *Theor. Chim. Acta* **94**, 311 (1996).
- <sup>69</sup>J. Delhalle, L. Piela, J.-L. Brédas, and J.-M. André, *Phys. Rev. B* **22**, 6254 (1980).
- <sup>70</sup>J.-Q. Sun and R. J. Bartlett, *Phys. Rev. Lett.* **80**, 349 (1998).
- <sup>71</sup>Orbital energy difference  $\epsilon_a - \epsilon_i$  gives the crudest estimate of the transition energy for the excitation  $a \leftarrow i$ . However, the orbital energy difference contains two-electron integrals such as  $(aa|ii)$  which may be regarded as self-interaction energy of an electron.
- <sup>72</sup>In the crystalline orbital calculations using periodic boundary conditions, an infinite one-dimensional lattice may be regarded as a ring of finite size. The number of unique wave vectors ( $K$ ) is equal to the number of unit cells in the ring, and is hence proportional to the size of the ring.
- <sup>73</sup>J. P. Perdew, R. G. Parr, M. Levy, and J. L. Balduz, Jr., *Phys. Rev. Lett.* **49**, 1691 (1982).
- <sup>74</sup>J. P. Perdew and M. Levy, *Phys. Rev. Lett.* **51**, 1884 (1983).
- <sup>75</sup>J. P. Perdew, *Int. J. Quantum Chem., Quantum Chem. Symp.* **19**, 497 (1986).
- <sup>76</sup>M. E. Casida, C. Jamorski, K. C. Casida, and D. R. Salahub, *J. Chem. Phys.* **108**, 4439 (1998).
- <sup>77</sup>D. J. Tozer and N. C. Handy, *J. Chem. Phys.* **109**, 10180 (1998).
- <sup>78</sup>P. W. Teare, *Acta Crystallogr.* **12**, 294 (1959).
- <sup>79</sup>M. Levy, J. P. Perdew, and V. Sahni, *Phys. Rev. A* **30**, 2745 (1984).
- <sup>80</sup>C.-O. Almbladh and U. von Barth, *Phys. Rev. B* **31**, 3231 (1985).
- <sup>81</sup>S. Hirata and R. J. Bartlett (unpublished).
- <sup>82</sup>J.-Q. Sun and R. J. Bartlett, *Phys. Rev. Lett.* **77**, 3669 (1996).
- <sup>83</sup>S. Ivanov, S. Hirata, and R. J. Bartlett (unpublished).